

Research on Transport and Mixing Dynamics of Valveless Piezoelectric Pump with Airfoil Baffles

XIONG Jian¹, KUANG Ming¹, WANG Lu², AFFANE Hiba¹, HUANG Yadong¹,
HUANG Jun^{1*}

1. Research Center of Fluid Machinery Engineering and Technology, Jiangsu University, Zhenjiang 212013, P. R. China;
2. Huaneng Gansu Energy Development Co. Ltd., Lanzhou 730070, P. R. China

(Received 19 February 2025; revised 1 April 2025; accepted 20 April 2025)

Abstract: To reduce the complexity of mixing systems and improve mixing efficiency, this paper proposes a valveless piezoelectric pump integrated with airfoil baffles, which embodies both active and passive mixing attributes. The airfoil baffles are designed using the asymmetric NACA63-412 profile. The impact of the airfoil angle of attack on the flow field within the tube and the output and mixing performance of the piezoelectric pump is investigated. Computational simulations of the tube with airfoil baffle indicated that as the angle of attack increases, the position of vortex generation at the leading and trailing edge regions of the airfoil baffle progressively moves forward in the direction of fluid flow. Then the vortex volume enlarges, and the vortex intensity within the flow field rises. Subsequently, the prototypes of valveless piezoelectric pumps at four different angles of attack are fabricated and their output performances are experimentally evaluated. The results demonstrate that the maximum output flow rate of the pump decreases with an increasing angle of attack. At an angle of attack of 0° , the maximum output flow rate of the pump reaches 225.3 ml/min. Mixing performance experiments are conducted using the piezoelectric pump for the synthesis of Fe_3O_4 particles. The findings indicate that as the angle of attack increases, the number of Fe_3O_4 particles formed in the mixture significantly rises, with a narrower particle size distribution and more regular morphology. At an angle of attack of 15° , the synthesized Fe_3O_4 particles have an approximate diameter of 10 μm . The outcomes of this paper offer valuable insights for the design of microfluidic systems, catering to the demands of material synthesis, chemistry, and biomedical applications.

Key words: micro mixer; airfoil baffle; piezoelectric pump; vortex; Fe_3O_4 particles

CLC number: TH38 **Document code:** A **Article ID:** 1005-1120(2025)02-0238-12

0 Introduction

With the advancement of microfluidic and microfabrication technologies, various microfluidic systems have been proposed and applied in fields such as chemical reactions^[1-3], medical detection^[4-6], and biology engineering^[7-9]. As a branch of microfluidic systems, micromixers play a crucial role in facilitating close contact between reactant molecules in chemical and biological reactions^[10-13]. Compared to macro-scale mixing systems, micromixers offer advantages such as fast reaction rates, high efficiency,

and minimal reagent consumption. Additionally, they feature simple structures, lower manufacturing costs, and easy integration with various detection systems.

Based on the differences in operating principles, micromixers can be classified into two types: Active micromixers and passive micromixers^[14-16]. Passive micromixers, based on their internal structures, are further categorized into multilayer laminar flow^[17] and chaotic advection micromixers^[18]. Cune-gatto et al.^[19] proposed a passive micromixer based on a Y-shaped flow channel with a multi-obstacle ar-

*Corresponding author, E-mail address: huangjun@ujs.edu.cn.

How to cite this article: XIONG Jian, KUANG Ming, WANG Lu, et al. Research on transport and mixing dynamics of valveless piezoelectric pump with airfoil baffles [J]. Transactions of Nanjing University of Aeronautics and Astronautics, 2025, 42(2): 238-249.

<http://dx.doi.org/10.16356/j.1005-1120.2025.02.008>

ray, which enhanced laminar flow disturbance by incorporating circular obstacles and grooves within the flow channel units. Similarly, Sun et al.^[20] proposed a passive micromixer based on Tesla/hexagonal flow channels, which achieved highly efficient mixing across a wide Reynolds number range within short mixing lengths by incorporating Ω -shaped and straight obstacles. Additionally, Sinha et al.^[21] developed a three-dimensional helical micromixer that induced secondary flow and chaotic advection through offset inlets and spiral channel geometry, achieving high-efficiency mixing across a Reynolds number within a range of 8—400.

Active micromixers involve placing movable components within microchannels or using external excitation to periodically disturb the flow field. This approach aims to increase the contact area between fluid microdomains or induce chaotic advection, thereby enhancing mixing efficiency. Active micromixers, depending on their driving mechanisms, can be categorized into piezoelectric-driven^[22], acoustic-driven^[23], magnetic-driven^[24] and electric field-driven^[25]. Generally, active micromixers exhibit higher mixing efficiency compared to passive micromixers. However, they are characterized by complex structures, high costs, and challenges such as thermal gradients that can potentially damage biological samples. As a result, these micromixers are not always the optimal choice for chemical and biological applications^[26]. Ward et al.^[27] pointed out that improving mixing methods could help utilize shorter channels. Therefore, they advocated combining active and passive mixing to leverage the advantages of both types. Deshmukh et al.^[28] integrated a micro-pulsation pump with a T-shaped micromixer to design a pressure-driven micromixer. This pulsation pump generated bubbles by heating the liquid, causing them to alternate between formation and collapse within the channel, thereby driving and stopping the flow intermittently to induce alternating fluid disturbances. Such velocity pulsations disrupted the fluid and increased their contact area, albeit at a lower driving frequency. Li et al.^[29] proposed a pulsation-based micromixer without using any dynamic chips outsideed, achieving uniform mixing. This mi-

cromixer consisted of an oscillator and a mixing unit, which utilizes a constant head pressure input to automatically generate pulsating pressure. Driven by pulsating pressure, periodic flow structures are generated within the mixing unit, promoting mixing within a short channel length. Wu et al.^[30] designed a micromixer composed of a microfluidic oscillator and a conical chamber. The oscillator included a small chamber with an elastic membrane that operated through a negative resistance mechanism. Under pressure driving into the fluid and exceeding the critical pumping pressure, the membrane underwent self-excited oscillations, converting the fluid into oscillating flow. This mechanism effectively stretched and folded the fluid to enhance mixing. Both of these mixers required an external driving pump, which reduced system integration.

Piezoelectric actuators driven by piezoelectric materials are characterized by rapid response, high energy density, immunity to electromagnetic interference, and ease of miniaturization^[31-34]. Therefore, researchers have developed numerous piezoelectric micro-pump-driven mixers. Lee et al.^[35] integrated a mixing region with a triangular structure into an obstacle-type valveless piezoelectric micro-pump for pumping and mixing solutions, achieving a maximum mixing index of 84%. Liu et al.^[36] proposed a multi-stage mixing micro-mixer driven by a valveless piezoelectric pump. Two valveless piezoelectric pumps were integrated into the micromixer, where the inlet and outlet microchannels of the micro-pumps were composed of diffuser/nozzle tubes and Tesla tubes. With a driving voltage of 60 V for a single micro-pump, the output flow rate was 0.20 ml/min. When the driving signals of the two piezoelectric pumps held a phase difference of 180°, the mixing efficiency at the outlet of the micromixer reached 99.39%. Subsequently, Yang et al.^[37] utilized this mixing system for the synthesis of nano-silver particles. Experimental results showed that as the driving voltage increased from 15 V to 60 V, the reaction performance of the mixing system gradually improved. The average particle size of AgNPs in the colloidal solution increased from 24.67 nm to 25.93 nm, and the concentration increased from

0.541 to 1.602. The introduction of such mixing systems has enhanced system integration. To further reduce complexity and improve mixing efficiency, our research group has developed a high-flow valveless piezoelectric pump with airfoil baffles^[38]. This pump utilized an airfoil-shaped structure as a baffle to achieve macroscopic unidirectional fluid output. The presence of the airfoil baffle generated a large vortex region within the flow channel. Coupled with the strong pulsation output characteristic of valveless piezoelectric pumps, this design may effectively enhance mixing efficiency.

Therefore, in this study, we develop a valveless piezoelectric mixing pump with airfoil baffles using the asymmetric NACA63-412 airfoil as the baffle structure. We investigate the transport and mixing performance of this valveless piezoelectric mixing pump using Fe_3O_4 micro particles as the synthesis target. First, computational fluid dynamics simulations are conducted on the flow field inside the tube containing an airfoil baffle to study the transient evolution characteristics of vortices, revealing the influence of airfoil angle of attack on the flow field dynamics. Second, experimental tests are performed on the output performance of the valveless piezoelectric mixing pump with airfoil baffles to analyze the impact of the airfoil angle of attack on the pump's output capabilities. Finally, Fe_3O_4 micro particle synthesis experiments are conducted using the valveless piezoelectric mixing pump. By analyzing the particle size and morphology of the synthesized particles, the mixing performance of the valveless piezoelectric mixing pump with airfoil baffles is evaluated. This study aims to provide a new perspective for the design of high-performance and easily integrable micro mixers, catering to application needs in fields such as material synthesis, chemistry, and biomedical sciences.

1 Working Principle and Structural Design

Ref.[38] reveals that when fluid flows along an airfoil baffle from the leading edge to the trailing edge (forward flow), the adverse pressure gradient

is small, preventing the occurrence of boundary layer separation. Separation may only occur at the trailing edge due to sudden expansion, resulting in lower flow resistance. When fluid flows from the trailing edge to the leading edge of the airfoil (reverse flow), boundary layer separation occurs after passing over the highest point of the airfoil surface, creating a low-pressure region. Consequently, the flow resistance during reverse flow is greater than that during forward flow. Fig.1 illustrates the valveless piezoelectric mixing pump with airfoil baffles. The piezoelectric vibrator vibrates in response to alternating voltage, causing periodic changes in the pump chamber volume. When the chamber volume increases, the internal pressure decreases, allowing external fluid to flow into the chamber through the inlet and outlet tubes under the influence of the pressure differential. This phase is regarded as the suction process of the piezoelectric pump. Conversely, as the chamber volume decreases, the internal pressure rises, forcing fluid to exit the chamber through the inlet and outlet tubes due to the pressure differential. This phase is known as the pumping process of the piezoelectric pump. Due to the unequal flow resistance experienced by fluid passing over the airfoil baffle in both forward and reverse directions, the flow rates of fluid entering and exiting the inlet and the outlet tubes during the suction and pumping processes of the piezoelectric pump are different. Therefore, with the vibration of the piezoelectric vibrator, the piezoelectric mixing pump can macroscopically generate a unidirectional pulsating output.

When the support and driving conditions of the piezoelectric vibrator are established, the flow resistance caused by the airfoil baffle in both forward and

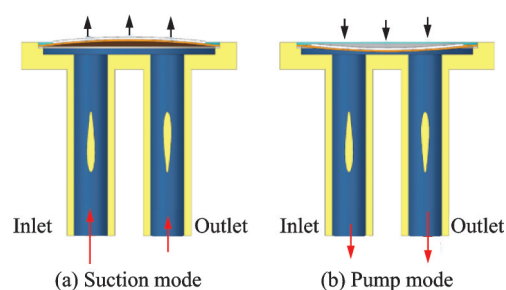


Fig.1 Schematic diagrams of a valveless piezoelectric pump with airfoil baffles

reverse directions will affect the output performance of the piezoelectric mixing pump.

The pressure loss coefficient (friction coefficient) for a tube with an airfoil is determined by

$$\xi = \frac{\Delta p}{\rho V^2 / 2} \quad (1)$$

where Δp represents the pressure difference across the tube with an airfoil; ρ the fluid density; and V the average flow velocity at the outlet of the tube. The outlet flow rate of the tube can be expressed as

$$q = A \left(\frac{2}{\rho} \right)^{1/2} \left(\frac{\Delta p}{\xi} \right)^{1/2} \quad (2)$$

where A is the cross-sectional area at the outlet of the tube with an airfoil.

According to Ref.[39], the output flow rate of the valveless piezoelectric mixing pump can be expressed as

$$V_0 = 2\Delta V \left[\frac{(\eta_{ba})^{1/2} - 1}{(\eta_{ba})^{1/2} + 1} \right] \quad (3)$$

$$\eta_{ba} = \frac{\xi_b}{\xi_a} \quad (4)$$

where f is the driving frequency of the piezoelectric vibrator; ΔV the volume change of the pump chamber when the vibrator moves to its highest position; η_{ba} the ratio of the flow resistance coefficients (impedance ratio) of the tube in forward and reverse directions; ξ_a the flow resistance coefficient in the forward direction and ξ_b the flow resistance coefficient in the reverse direction. Eq.(3) indicates that $\xi_a \neq \xi_b$, allowing the piezoelectric mixing pump to transport fluid in a unidirectional manner.

As the angle of attack of the airfoil changes, the intensity and spatial distribution of vortical structures vary within the flow field in the tube, thereby influencing the transport and mixing performance of the valveless piezoelectric mixing pump with airfoil baffles. To investigate this, the asymmetric airfoil NACA63-412 is chosen as the baffle, and four valveless piezoelectric mixing pumps are designed with airfoil angles of 0° , 5° , 10° , and 15° as the attack angles. The pump mainly consists of inlet and outlet tubes with an airfoil, a pump chamber, a cover plate, and a piezoelectric vibrator, as shown in Fig.2.

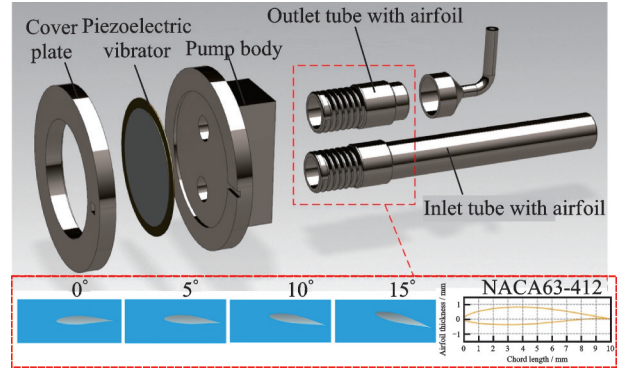


Fig.2 Assembly schematic of valveless piezoelectric mixing pump with airfoil baffles

2 Flow Field Simulation

To study the transient evolution characteristics of vortices in the flow field within the tube and elucidate the influence of airfoil angle of attack on vortex structure intensity and spatial distribution, transient numerical simulations of the flow field in the tube are conducted by COMSOL software. Four different models of the tubes with asymmetric airfoil NACA63-412 at angles of attack of 0° , 5° , 10° , and 15° are established. The airfoil baffle has a chord length of 10 mm, and the inner diameter of the tube is 8 mm. The simulation medium is liquid water with a density of $1\ 000\ \text{kg/m}^3$ and a dynamic viscosity of $1 \times 10^{-3}\ \text{Pa}\cdot\text{s}$. At the inlet boundary, a velocity boundary condition is applied, set as pulsatile velocity with a frequency of 42 Hz. The SIMPLE algorithm is employed to solve the coupled equations for flow field velocity and pressure.

Considering the accuracy of the computational results and the computational load, a detailed examination of the computational domain grid is conducted. Validation is performed using grid cell counts of 2.1 million, 2.5 million, 2.9 million, 3.3 million, and 3.5 million. The net output flow rates computed with 3.5 million grid cells are compared with those with 2.1 million, 2.5 million, 2.9 million, and 3.3 million grid cells, resulting in ratios of 94.2%, 97.5%, 98.6%, and 99.3%, respectively. These results are shown in Fig.3. Considering both computational time and accuracy, a grid cell count of approximately 3.3 million is selected for the flow field simulations.

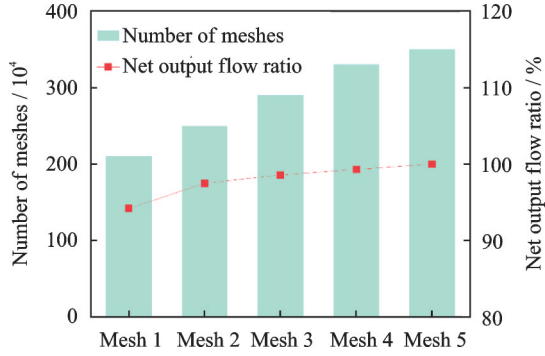


Fig.3 Grid independence validation results

Helicity is an important physical quantity that measures the topology of turbulent vortices in a flow field. Therefore, a method based on regularized helicity is employed to identify the distribution of vortices within the tube and to study the transient evolution characteristics of these vortices. Regularized helicity is defined as the dot product of velocity and vorticity, divided by the product of the magnitudes of velocity and vorticity. The expression is given by

$$H_n = \frac{\mathbf{V} \cdot \boldsymbol{\omega}}{|\mathbf{V}| \cdot |\boldsymbol{\omega}|} \quad (5)$$

where \mathbf{V} represents the velocity vector and $\boldsymbol{\omega}$ the vorticity vector. The normalized helicity H_n ranges between -1 and 1 . In the vortex core region of the flow field, the direction of the velocity vector tends to align with the direction of the vorticity vector, the value of H_n tends towards ± 1 . The sign of H_n indicates the direction of rotation of the vortex: If H_n is positive, the vortex rotates counterclockwise relative to the flow direction; if H_n is negative, the vortex rotates clockwise relative to the flow direction. The larger the absolute value of H_n , the stronger the intensity of the vortex.

3 Experimental Setup

The pump body and tube containing the airfoil baffle are manufactured using Stereolithography (SLA) 3D printing technology with photosensitive resin. The piezoelectric vibrator used in the experiment is a composite circular plate type made from PZT-5A material. The structural parameters of the pump body and the piezoelectric vibrator for the piezoelectric mixing pump are shown in Table 1.

Table 1 Structural parameters of the piezoelectric mixing pump

Parameter	Chamber diameter	Chamber depth	Vibrator diameter	Vibrator thickness
Value	40	4	45	0.5

The vibrator of a piezoelectric pump is tested by a laser Doppler vibrometer (PSV-300F-B, Polytec Ltd., Germany) in a swept-frequency experiment to determine its resonant frequency corresponding to the first-order bending vibration mode. The output performance tests of the valveless piezoelectric mixing pump with airfoil baffles include experiments on output flow rate and output back pressure. The schematic of the output performance experiment is shown in Fig.4. A signal generator and power amplifier provide a driving voltage of 100 V to excite the piezoelectric vibrator, and the output of the piezoelectric pump is controlled by adjusting the driving frequency. To measure the output flow rate under zero back pressure conditions, a balance is used to weigh the mass of liquid output per unit time, yielding a curve of output flow rate versus frequency variation. Under maximum flow rate conditions, the output flow rate of the pump is tested at different driving voltages by adjusting the driving voltage of the piezoelectric vibrator. Subsequently, an L-shaped tube is connected at the pump outlet to record the difference in liquid levels between the outlet and inlet under different driving frequencies, generating a curve of output back pressure versus frequency variation. All output performance tests of the piezoelectric mixing pump use deionized water as the working fluid.

This study employs co-precipitation to prepare Fe_3O_4 particles and characterizes their morphology and particle size to assess the mixing performance of the valveless piezoelectric pump with airfoil baffles. The required solutions for the experiment consist of FeCl_3 , FeSO_4 , and saturated NaOH solution. The reaction principle is



FeCl_3 and FeSO_4 solutions are mixed in a 1:1 ratio, and the solution concentrations include FeCl_3 (0.1 M), FeSO_4 (0.05 M), NaOH (1.5 M), fol-

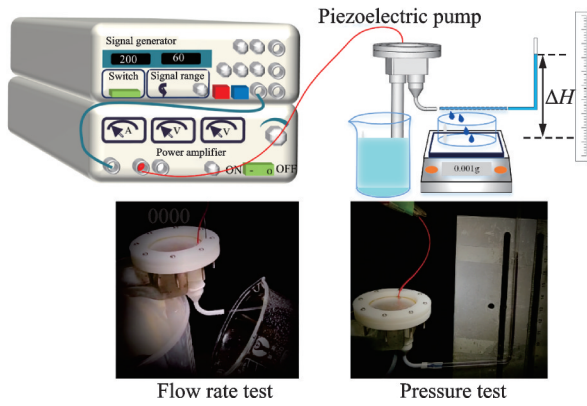


Fig.4 Output performance experiment

lowed by the addition of saturated NaOH solution to achieve mixed solution of $\text{pH} > 9$. Subsequently, distilled water is added to prepare the mixed solution. Using valveless piezoelectric mixing pumps with different angles of attack of the airfoil, circulation mixing and pumping experiments are conducted for 15 min. The temperature is $25\text{ }^\circ\text{C}$ (room temperature, controlled). The piezoelectric pump operates at 100 V , 42 Hz (resonant frequency), while the magnetic stirrer operates at $1\text{ }000\text{ r/min}$. Finally, samples are directly taken from the mixed solution, and the morphology of the generated particles is observed using a scanning electron microscope (Kath-Matic, KS-X1500) for their characteristics. Image processing is then performed to analyze the particle size distribution. The flowchart of the mixing experiment is shown in Fig.5. Simultaneously, a magnetic stirrer is used to stir the mixed solution (FeCl_3 , FeSO_4 , and saturated NaOH solution) to obtain microparticle products which serve as the control group for comparative evaluation of the mixing performance of the airfoil-based valveless piezoelectric mixing pump.

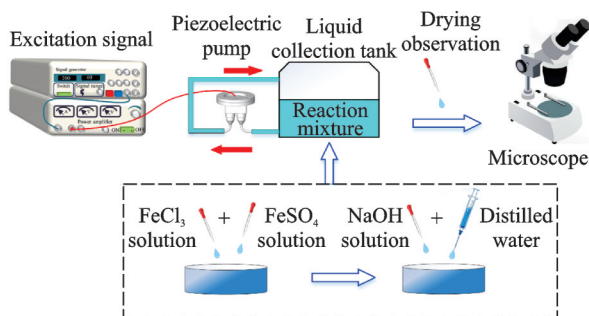


Fig.5 Flow chart of mixing experiment

4 Results and Discussion

At four characteristic instants within one velocity cycle, the results of the flow field computations are selected. Vortex identification using regularized helicity reveal the distribution of vortex iso-surfaces, as shown in Fig.6. At time 0, when the fluid flows forward over the airfoil, vortices predominantly form near the leading and trailing edges of the airfoil. Particularly, symmetric vortices of approximately equal size and opposite rotation directions are generated near the wall surface of the tube. At $T/4$, when the fluid velocity reaches its peak in the forward direction, vortices near the leading edges of the airfoil and close to the walls of the tube further evolve, forming multiscale vortex structures. Particularly, smaller vortices initially present near the upper and lower surfaces of the airfoil near the trailing edge and adjacent to the walls of the tube undergo further development. This results in the generation of numerous multiscale vortex structures and their shedding, with the volumes of these vortex structures decreasing along the direction of fluid flow. At $T/2$, when the fluid starts to flow in reverse over the airfoil, symmetric vortices of equal scale and opposite rotation directions are observed near the trailing edge of the airfoil and adjacent to the walls of the tube. However, the volumes of vortices on the upper and the lower surfaces of the airfoil are different. Fewer vortices are generated in the region near the leading edge of the airfoil. At $3T/4$, when the fluid velocity reaches its peak in reverse flow, multiscale vortex systems are observed near the upper and the lower surfaces of the airfoil near the trailing edge and adjacent to the walls of the tube. These vortex systems primarily migrate and develop along the axial direction. In the region near the leading edge of the airfoil, the distribution of vortex systems is more complex. The shedding vortices from the trailing edge interact with the vortices generated in the leading edge region, forming multiscale complex vortex systems. Moreover, the total volume of vortex systems on the lower surface of the airfoil baffle is larger than that on the upper surface.

From Fig.6, it is evident that vortices in the

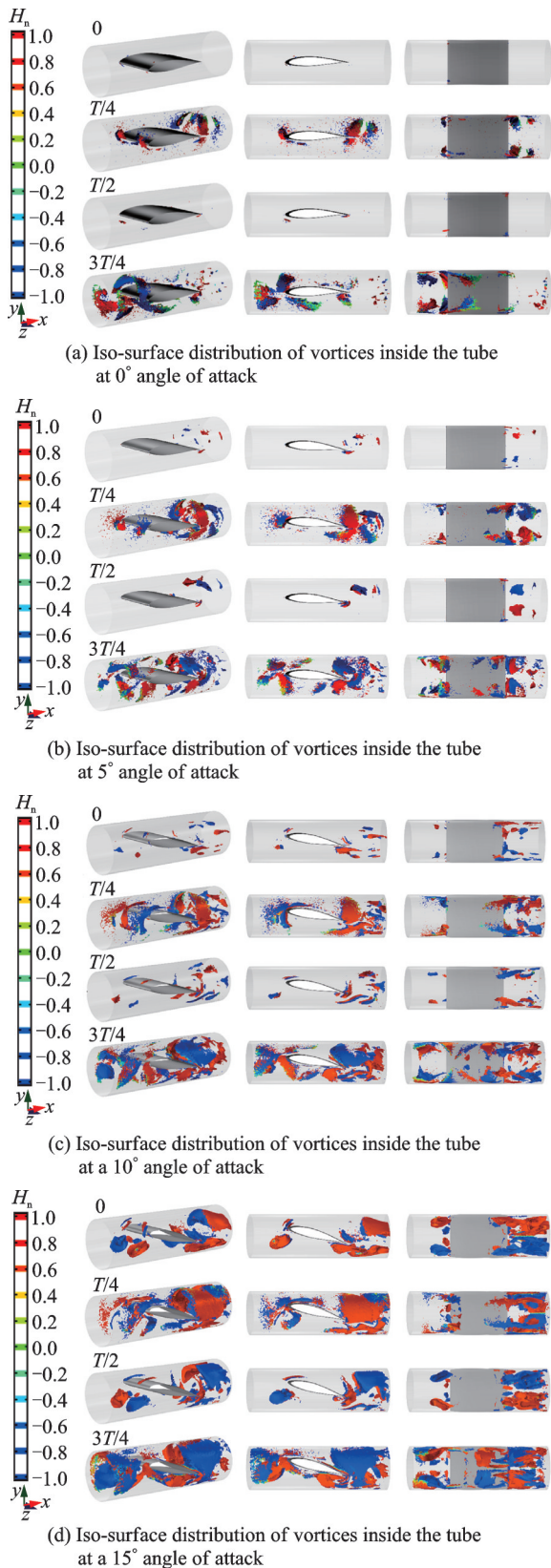


Fig.6 Iso-surface distribution of vortices inside a tube with an airfoil baffle

flow field mainly form near the leading and trailing edges of the airfoil. The size and position of these vortices vary with time, and interactions between

vortices at different locations result in multiscale complex vortex systems. Over one cycle, as the angle of attack increases and the fluid flows forward and then reverses over the airfoil, the positions where vortices form near the leading and trailing edges of the airfoil gradually move forward along the direction of fluid flow, and their volumes increase progressively. Additionally, the symmetry of vortices and the shedding phenomenon become more pronounced, indicating that the angle of attack significantly influences the formation and development of vortices. Next is the enhancement of unidirectional pulsation by vortex dynamics. As shown in Fig.6, the transient evolution of vortices within the flow field further amplifies the asymmetry of the resistance to forward and reverse flows. In the forward flow phase, small-scale vortices predominantly form near the trailing edge of the guide vane, exhibiting periodic shedding with lower energy dissipation. Here, fluid energy is primarily directed toward driving outflow. In the reverse flow phase, during backflow, a large-scale vortex develops near the leading edge of the guide vane due to the adverse pressure gradient. The generation, migration, and interaction of these vortices induce intense turbulent mixing, leading to significantly increased energy losses, thereby suppressing reverse flow. And the simulations reveal that as the attack angle increases, both the vortex intensity and spatial asymmetry intensify.

Fig.7 shows the regularized helicity curves of the flow field vortices. A larger absolute value of H_n indicates stronger vortices. It can be seen from Fig.7 that as the angle of attack increases, the strength of

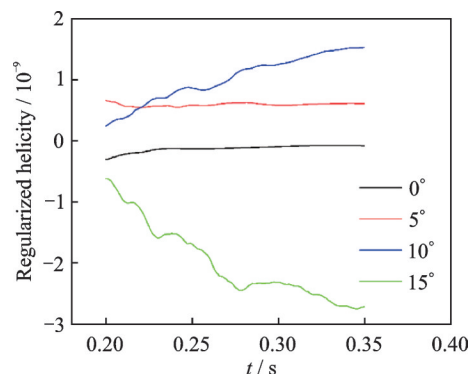


Fig.7 Regularized vorticity curves of the flow field

the flow field vortices also increases.

Fig.8 presents the vibration test results of the piezoelectric vibrator. The results indicate that the first-order bending resonance frequency of the piezoelectric vibrator used in this pump is 158.5 Hz under no-load conditions (without fluid or tubing connections).

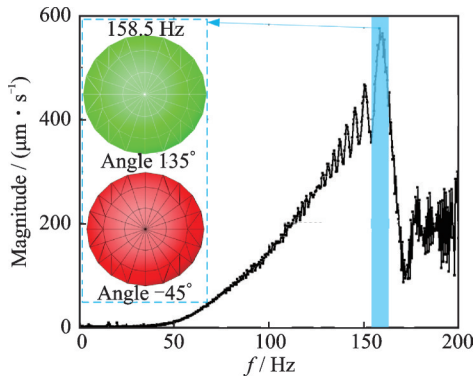


Fig.8 Vibration test results of the piezoelectric vibrator

Fig.9 shows the output performance curves of valveless piezoelectric mixing pumps with different angles of attack airfoil baffles. Fig.9(a) depicts the flow rate-frequency curves. It can be observed that the maximum output flow rate of the piezoelectric mixing pump decreases gradually with an increasing angle of attack of the airfoil baffle. At 0° angle of attack, the maximum output flow rate of the valveless piezoelectric mixing pump with airfoil baffles is 225.3 ml/min. Fig.9(b) shows the flow rate-voltage curves of the valveless piezoelectric mixing pump at its optimal operating point. As the driving voltage increases, the output flow rate of the piezoelectric pump also increases. At a driving voltage of 110 V, the output flow rate of the valveless piezoelectric mixing pump with 0° angle of attack airfoil baffles reaches 242.52 ml/min. Fig.9(c) shows the output backpressure-frequency curves of the valveless piezoelectric mixing pump with the airfoil baffles. It can be observed that as the angle of attack of the airfoil baffle increases, the output backpressure of the piezoelectric mixing pump decreases, and the frequency at which maximum output backpressure occurs also decreases with an increasing angle of attack. At 0° angle of attack, the maximum output backpressure of the valveless piezoelectric mixing pump with the airfoil baffles is 813.2 Pa.

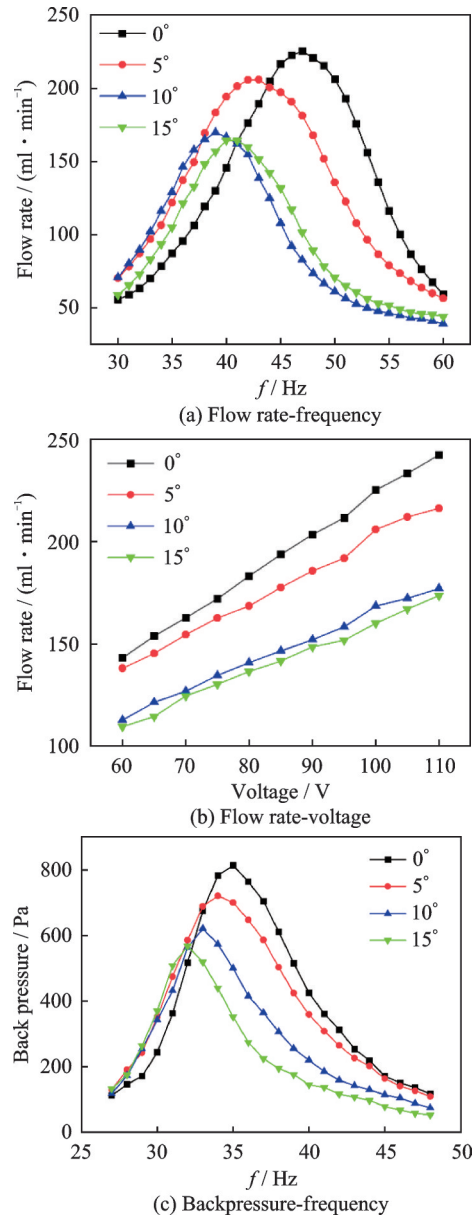


Fig.9 Output performance curves of the valveless piezoelectric mixing pump

The experimental results in Figs.8, 9 indicate that the optimal operating frequency of the piezoelectric pump (the frequency corresponding to peak flow rate) differs significantly from the no-load resonance frequency of the vibrator. Specifically, during the output performance tests, the addition of inlet/outlet tubing and working fluid substantially increases the system's equivalent mass and alters its mechanical impedance, leading to a reduction in the resonant frequency. Consequently, the optimal operating frequency for maximum flow rate (42 Hz at 0° angle of attack) is notably lower than the first-order bending resonance frequency of the piezoelectric vibrator (158.5 Hz).

This study also compares the output flow rate of the proposed piezoelectric pump with existing piezoelectric pump-driven micromixers, as summarized in Table 2. The results demonstrate that at a driving voltage of 100 V, the pump achieves a maximum output flow rate of 225.3 ml/min at 0° angle of attack, significantly outperforming comparable devices. This highlights the pump's superior capability for high-flow applications.

Table 2 Flow rate comparison of different piezoelectric pump-driven micromixers

Study	Voltage/V	Flow rate/(ml·min ⁻¹)
Liu et al. ^[36]	60	0.2
Lee et al. ^[35]	40	0.156
This work	100	225.3

Fig.10 shows micrographs of the reaction solution after 15 min of mixing. Specifically, Fig.10(a) depicts the micrograph of the mixture stirred with a magnetic stirrer. Figs.10(b—e) show micrographs of the mixture after mixing using valveless piezoelectric mixing pumps with airfoil baffles at different angles of attack.

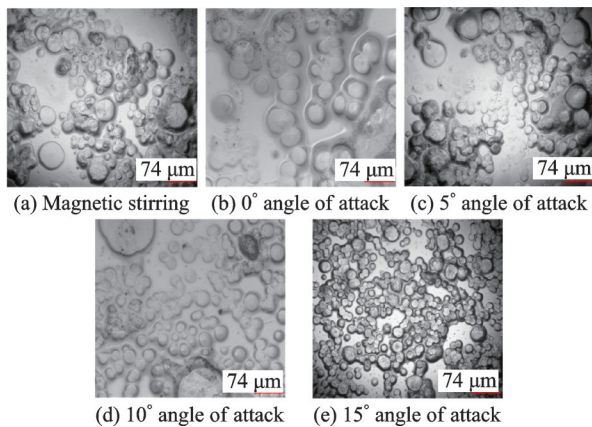


Fig.10 Micrographs of the mixed solution

To further quantitatively analyze the size and quantity of the generated Fe₃O₄ particles, we introduce the Feret diameter concept, which measures the diameter passing through the center of a particle in any direction. We perform edge-based image segmentation on the micrographs of the particles, as depicted in Fig.11. Subsequently, based on the results of image processing, we measure the diameters and count the particles to obtain the Feret diameter dis-

tribution of the Fe₃O₄ particles, as shown in Fig.12. Figs.11, 12, show that at 0° angle of attack, the Fe₃O₄ particles generated by the piezoelectric mixing pump have a diameter predominantly around 50 μm, with irregular shapes and relatively few in number. At 5° angle of attack, the particle diameter is approximately 30 μm, showing slight improvement in both diameter and shape, with an increased number of Fe₃O₄ particles, though the diameter distribution is wider. With 10° angle of attack, the Fe₃O₄ particles in the mixture have a diameter of around 20 μm, exhibiting more regular shapes and a significant increase in quantity. At 15° angle of attack, the particle diameter distribution ranges around 10 μm, with regular shapes and a sharp increase in particle quantity. In contrast, the generated particles using a magnetic stirrer exhibit a wider diameter range from 10 μm to 70 μm, with a broader distribution. Furthermore, both the morphology and quantity of the generated particles are notably inferior compared to those generated by the piezoelectric mixing pump at 15° angle of attack.

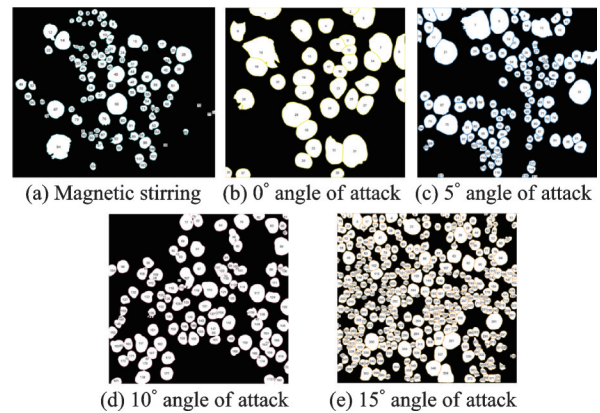


Fig.11 Processed images of Fe₃O₄ particles

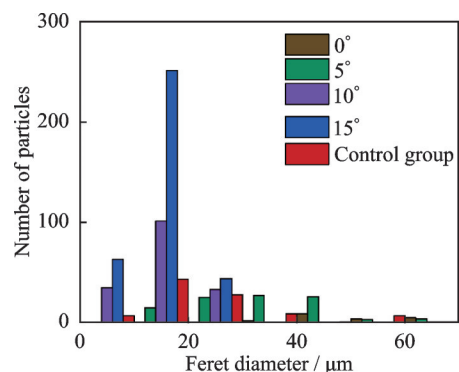


Fig.12 Feret diameter distribution of Fe₃O₄ particles

5 Conclusions

We utilize the asymmetric airfoil NACA63-412 as a baffle to construct a valveless piezoelectric mixing pump and investigate the influence of varying angles of attack on the flow field inside the tube and the output performance of the piezoelectric pump. Simulation results indicate that with increasing angle of attack, the positions where vortices are generated around the leading edge and trailing edge of the airfoil shift forward along the flow direction, and their volumes gradually increase. Additionally, the symmetry and shedding phenomena of the vortices become more pronounced, leading to increased vortex intensity in the flow field, which effectively enhances mixing efficiency. Experimental results on the output performance of the piezoelectric pump show that as the angle of attack increases, the maximum output flow rate gradually decreases. Specifically, at 0° angle of attack, the maximum output flow rate of the valveless piezoelectric mixing pump with the airfoil baffles is 225.3 ml/min, with a maximum output backpressure of 813.2 Pa. Using Fe_3O_4 microparticles as the synthesis target, experiments are conducted on the mixing performance of the valveless piezoelectric mixing pump with airfoil baffles. The results indicate that with an increasing angle of attack, the number of Fe_3O_4 particles generated in the mixture significantly increases, resulting in a narrower particle size distribution and more regular particle morphology. The proposed valveless piezoelectric mixing pump with airfoil baffles exhibits excellent output and mixing performance. This pump shows promising applications in material synthesis, chemistry, and biomedical fields, enhancing system integration and improving mixing efficiency.

References

- [1] DEMELLO A J. Control and detection of chemical reactions in microfluidic systems[J]. *Nature*, 2006, 442(7101): 394-402.
- [2] SRIVASTAVA K, BOYLE N D, FLAMAN G T, et al. In situ spatiotemporal characterization and analysis of chemical reactions using an ATR-integrated microfluidic reactor[J]. *Lab on a Chip*, 2023, 23(21): 4690-4700.
- [3] NICULESCU A G, MUNTEANU MIHAIESCU O M, BÎRCĂ A C, et al. New 3D vortex microfluidic system tested for magnetic core-shell Fe_3O_4 -SA nanoparticle synthesis[J]. *Nanomaterials*, 2024, 14(11): 902.
- [4] LAPIZCO-ENCINAS B H, ZHANG Y V. Microfluidic systems in clinical diagnosis[J]. *Electrophoresis*, 2023, 44(1/2): 217-245.
- [5] XIANG Y, HU C, WU G, et al. Nanomaterial-based microfluidic systems for cancer biomarker detection: Recent applications and future perspectives[J]. *TrAC Trends in Analytical Chemistry*, 2023, 158: 116835.
- [6] SURAPPA S, MULTANI P, PARLATAN U, et al. Integrated "lab-on-a-chip" microfluidic systems for isolation, enrichment, and analysis of cancer biomarkers[J]. *Lab on a Chip*, 2023, 23(13): 2942-2958.
- [7] BANIK S, UCHIL A, KALSANG T, et al. The revolution of PDMS microfluidics in cellular biology[J]. *Critical Reviews in Biotechnology*, 2023, 43(3): 465-483.
- [8] TOLABI H, DAVARI N, KHAJEHMOHAMMADI M, et al. Progress of microfluidic hydrogel-based scaffolds and organ-on-chips for the cartilage tissue engineering[J]. *Advanced Materials*, 2023, 35(26): e2208852.
- [9] ENDERS A, GRÜNBERGER A, BAHNEMANN J. Towards small scale: Overview and applications of microfluidics in biotechnology[J]. *Molecular Biotechnology*, 2024, 66(3): 365-377.
- [10] LIU C, LI Y, LIU B F. Micromixers and their applications in kinetic analysis of biochemical reactions[J]. *Talanta*, 2019, 205: 120136.
- [11] JEONG G S, CHUNG S, KIM C B, et al. Applications of micromixing technology[J]. *Analyst*, 2010, 135(3): 460-473.
- [12] RAZAVI BAZAZ S, SAYYAH A, HAZERI A H, et al. Micromixer research trend of active and passive designs[J]. *Chemical Engineering Science*, 2024, 293: 120028.
- [13] WANG X, LIU Z Q, WANG B, et al. An overview on state-of-art of micromixer designs, characteristics and applications[J]. *Analytica Chimica Acta*, 2023, 1279: 341685.
- [14] LEE C Y, WANG W T, LIU C C, et al. Passive mixers in microfluidic systems: A review[J]. *Chemical Engineering Journal*, 2016, 288: 146-160.
- [15] HESSEL V, LÖWE H, SCHÖNFELD F. Micromixers: A review on passive and active mixing principles[J]. *Chemical Engineering Science*, 2005, 60(8/9): 2479-2501.

- [16] MOUSAVI S M, AALAEI E, RAD H S, et al. Numerical study of the performance of an active micromixer based on the oscillations of a microbeam[J]. *Chemical Engineering Science*, 2024, 297: 120273.
- [17] LOTFIANI A, REZAZADEH G. A new two-layer passive micromixer design based on SAR-vortex principles[J]. *International Journal of Chemical Reactor Engineering*, 2021, 19(3): 309-329.
- [18] AHMAD ANSARI M, KIM K Y, ANWAR K, et al. A novel passive micromixer based on unbalanced splits and collisions of fluid streams[J]. *Journal of Micromechanics and Microengineering*, 2010, 20(5): 055007.
- [19] CUNEGATTO E H T, ZINANI F S F, BISERNI C, et al. Constructal design of passive micromixers with multiple obstacles via computational fluid dynamics[J]. *International Journal of Heat and Mass Transfer*, 2023, 215: 124519.
- [20] SUN J J, SHI Z Q, ZHONG M J, et al. Numerical and experimental investigation on a planar passive micromixer embedded with omega-shaped obstacles for rapid fluid mixing[J]. *Chemical Engineering and Processing-Process Intensification*, 2022, 182: 109203.
- [21] SINHA A, ZUNAID M. Numerical study of passive mixing in a 3-dimensional helical micromixer with two inlets at offset[J]. *Materials Today: Proceedings*, 2022, 56: 3676-3681.
- [22] LIU Guojun, ZHAO Tian, WANG Conghui, et al. Optimization of structure and working parameters of Y type micro-mixer in two-phase pulsating mixing[J]. *Journal of Jilin University (Engineering and Technology Edition)*, 2015, 45(4): 1155-1161.(in Chinese)
- [23] BEZAGU M, ARSENIYADIS S, COSSY J, et al. A fast and switchable microfluidic mixer based on ultrasound-induced vaporization of perfluorocarbon[J]. *Lab on a Chip*, 2015, 15(9): 2025-2029.
- [24] WEN C Y, YE H C P, TSAI C H, et al. Rapid magnetic microfluidic mixer utilizing AC electromagnetic field[J]. *Electrophoresis*, 2009, 30(24): 4179-4186.
- [25] ODDY M H, SANTIAGO J G, MIKKELSEN J C. Electrokinetic instability micromixing[J]. *Analytical Chemistry*, 2001, 73(24): 5822-5832.
- [26] CAPRETTO L, CHENG W, HILL M, et al. Micromixing within microfluidic devices[M]//*Microfluidics*. Berlin, Heidelberg: Springer, 2011: 27-68.
- [27] WARD K, HUGH FAN Z. Mixing in microfluidic devices and enhancement methods[J]. *Journal of Micromechanics and Microengineering*, 2015, 25(9): 094001.
- [28] DESHMUKH A A, LIEPMANN D, PISANO A P. Continuous micromixer with pulsatile micropumps[C]//*Proceedings of 2000 Solid-State, Actuators, and Microsystems Workshop Technical Digest*. Hilton Head, USA: Transducer Research Foundation, Inc., 2000: 73-76.
- [29] LI Z L, KIM S J. Pulsatile micromixing using water-head-driven microfluidic oscillators[J]. *Chemical Engineering Journal*, 2017, 313: 1364-1369.
- [30] WU J W, XIA H M, ZHANG Y Y, et al. An efficient micromixer combining oscillatory flow and divergent circular chambers[J]. *Microsystem Technologies*, 2019, 25(7): 2741-2750.
- [31] LI N, FEI P, TOUS C, et al. Human-scale navigation of magnetic microrobots in hepatic arteries[J]. *Science Robotics*, 2024, 9(87): eadh8702.
- [32] HUANG J, YANG J L, LI L J, et al. The aggregation of micro-particles based on hydraulic vortices[J]. *Physics of Fluids*, 2024, 36(3): 032005.
- [33] HUANG Jun, ZHU Yichao, SHI Weidong, et al. Design of cymbal shape slotted valve based piezoelectric pump[J]. *Optics and Precision Engineering*, 2017, 25(11): 2914-2922. (in Chinese)
- [34] SHI Y L, LI N, TREMBLAY C C, et al. A piezoelectric robotic system for MRI targeting assessments of therapeutics during dipole field navigation[J]. *IEEE/ASME Transactions on Mechatronics*, 2021, 26(1): 214-225.
- [35] LEE C J, SHEEN H J, TU Z K, et al. A study of PZT valveless micropump with asymmetric obstacles[J]. *Microsystem Technologies*, 2009, 15(7): 993-1000.
- [36] LIU G J, WANG M, LI P F, et al. A micromixer driven by two valveless piezoelectric pumps with multi-stage mixing characteristics[J]. *Sensors and Actuators A: Physical*, 2022, 333: 113225.
- [37] YANG Z G, DONG L T, WANG M, et al. Controllable synthesis of silver nanoparticles using a multi-stage microfluidic reactor driven by two valveless piezoelectric pumps[J]. *Sensors and Actuators A: Physical*, 2022, 346: 113871.
- [38] WANG L, YANG J L, AFFANE H, et al. A high flow-rate single-chamber valveless piezoelectric pump with airfoil baffles[J]. *Sensors and Actuators A: Physical*, 2023, 354: 114229.
- [39] STEMME E, STEMME G. A valveless diffuser/nozzle-based fluid pump[J]. *Sensors and Actuators A: physical*, 1993, 39(2): 159-167.

Acknowledgements This work was supported by the National Natural Science Foundation of China (Nos.

51605200, 52206045).

Authors

The first author Mr. XIONG Jian received his bachelor's degree in power machinery and automation from School of Automotive and Traffic Engineering, Jiangsu University in 2022. He is currently a postgraduate at Jiangsu University. His research interests include the flow field simulation of piezoelectric micropump and the hybrid application of micro particles.

The corresponding author Dr. HUANG Jun received his M.E. degree in nuclear technology and application and Ph.D. degree in mechanical design and theory from Nanjing University of Aeronautics and Astronautics, Nanjing, China, in 2009 and 2014, respectively. He is currently an associate professor with Research Center of Fluid Machinery Engineering and Technology, Jiangsu University. His research interests include piezoelectric actuators and sensors.

Author contributions Mr. XIONG Jian carried out the

prototype fabrication and all experimental work, processed the flow field simulation results, and supplied key data for the manuscript. Mr. KUANG Ming helped with the microparticle synthesis experiments, collected and processed experimental data, and verified the accuracy of the results. Mr. WANG Lu developed the flow field simulation model and performed the computational analysis. Ms. AFFANE Hiba assisted in the statistical and analytical work of the experimental and flow field simulation results and contributed to the research background and current status. Dr. HUANG Ya-dong assisted in analyzing the flow field simulation results, validated the findings, and provided insights for the discussion. Dr. HUANG Jun designed the study, developed and conducted the analysis, interpreted the results, and drafted the manuscript. All authors commented on the manuscript draft and approved the submission.

Competing interests The authors declare no competing interests.

(Production Editor: ZHANG Bei)

翼型挡体无阀压电混合泵传输和混合特性研究

熊健¹, 邝铭¹, 王璐², AFFANE Hiba¹, 黄亚冬¹, 黄俊¹

(1. 江苏大学流体机械工程技术研究中心, 镇江 212013, 中国;

2. 华能甘肃能源开发有限公司, 兰州 730070, 中国)

摘要: 为了降低混合系统的复杂性、提高混合效率, 以非对称翼型 NACA63-412 为挡体, 提出了具有主动混合与被动混合特点的翼型挡体无阀压电混合泵。研究了翼型迎角变化对流管内流场和压电混合泵输出、混合性能的影响。对含翼型流管进行了流场模拟, 结果表明, 随翼型迎角的增大, 当流体分别以正向和反向流经翼型挡体时, 涡旋在翼型的前缘区域与尾缘区域的形成位点会随着流体流动方向的改变而逐步向前迁移。体积逐渐增大, 且流场涡旋强度增大。随后, 制作了 4 种不同迎角的翼型挡体无阀压电混合泵样机并进行了输出性能试验。结果表明, 随翼型迎角的增大, 压电混合泵的最大输出流量逐渐减小。当翼型迎角为 0° 时, 翼型挡体无阀压电混合泵的最大输出流量为 225.3 ml/min。以 Fe₃O₄ 微颗粒为合成对象, 利用翼型挡体无阀压电混合泵进行了混合性能试验。结果表明: 随翼型迎角的增大, 混合液内生成的 Fe₃O₄ 粒子数量明显增加, 粒径分布变窄, 且粒子形貌越发规则。当翼型迎角为 15° 时, 生成的 Fe₃O₄ 粒子粒径约为 10 μm。该研究结果可为微流控系统的设计提供有效参考, 满足材料合成、化学和生物医学等领域的应用需求。

关键词: 微混合器; 翼型挡体; 压电泵; 涡旋; Fe₃O₄ 粒子